Available online at www.sciencedirect.com

ScienceDirect

Ceramics International 41 (2015) 3901–3909

CERAMICS INTERNATIONAL

www.elsevier.com/locate/ceramint

Properties of CMAS glass from desert sand

Narottam P. Bansal[a,*], Sung R. Choi[b]

[a]Materials and Structures Division, NASA Glenn Research Center, Cleveland, OH 44135, USA
[b]Naval Air Systems Command, Patuxent River, MD 20670, USA

Received 18 September 2014; received in revised form 12 November 2014; accepted 13 November 2014
Available online 21 November 2014

Abstract

X-ray diffraction analysis of as-received desert sand from a Middle East country showed the presence of quartz (SiO_2), calcite ($CaCO_3$), gypsum ($CaSO_4.2H_2O$), $NaAlSi_3O_8$, $Mg_2(Al_{3.9}Si_{5.1}O_{18})$ and $Mg_3Al_2(SiO_4)_3$ phases. A batch of as-received desert sand was melted into calcium magnesium aluminosilicate (CMAS) glass at ~1500 °C. From inductively coupled plasma-atomic emission spectrometry, chemical composition of the CMAS glass was analyzed to be 27.8CaO-4MgO-5Al_2O_3-61.6SiO_2-0.6Fe_2O_3-1K_2O (mole %). Various physical, thermal, and mechanical properties of the glass have been evaluated. Bulk density of CMAS glass was 2.69 g/cm^3, Young's modulus 92 GPa, Shear modulus 36 GPa, Poisson's ratio 0.28, dilatometric glass transition temperature (T_g) 706 °C, softening point (T_d) 764 °C, Vickers microhardness 6.3 ± 0.4 GPa, indentation fracture toughness 0.75 ± 0.15 MPa.m$^{1/2}$, and coefficient of thermal expansion (CTE) 9.8 × 10^{-6}/°C in the temperature range 25 to 700 °C. Temperature dependence of viscosity has also been estimated from various reference points of the CMAS glass using the Vogel-Fulcher-Tamman (VFT) equation as well as from the glass composition. The glass remained amorphous after heat treating at 850 °C for 10 h but crystallized into $CaSiO_3$ and $Ca_2Mg_{0.5}AlSi_{1.5}O_7$ phases at 900 °C or higher temperatures. Crystallization kinetics of the CMAS glass has also been investigated by differential thermal analysis (DTA).
Published by Elsevier Ltd and Techna Group S.r.l.

Keywords: CMAS; Mechanical properties; Thermal properties; Crystallization; Viscosity

1. Introduction

Ingested particulate materials such as sand, fly ash and volcanic ash may cause serious damage by erosion as it passes through the jet engine or by plugging the cooling holes of the combustor liner and the blades resulting in premature failure. To improve efficiency, future jet engines will operate at higher temperatures than the current engines. SiC fibers-reinforced SiC matrix (SiC_f/SiC) composites are being developed for hot section components (combustor liner, vanes, blades, etc.) of next generation turbine engines for operation at temperatures of 2700–3000 F (1482–1649 °C). The gas temperatures will be even higher than the surface temperatures. At these elevated operating temperatures, desert sand or runway dust ingested into turbine engines will fully decompose and melt into a viscous and corrosive slag-like material of calcium magnesium aluminosilicate (CMAS) composition. Molten CMAS may chemically interact and/or infiltrate into the pores of thermal and environmental barrier coatings (TBC/EBC) and may deposit on the surfaces of various engine components [1–6]. During cooling cycle of the engine unreacted CMAS will convert into glass. CMAS damage of TBCs mostly occurs from thermomechanical reasons and degradation of EBCs due to thermochemical interactions. These processes could adversely affect the performance and life of jet engines. To help understand the effects of CMAS on durability of TBCs and EBCs, it would be beneficial if various properties of the desert sand glass are available.

The objective of the current study was to characterize the as-received desert sand from a Middle East country for its composition and thermal stability and also to evaluate the various physical, thermal, and mechanical properties of the CMAS glass resulting from melting of the desert sand.

*Corresponding author. Tel.: +1 216 433 3855; fax: +1 216 433 5544.
E-mail address: narottam.p.bansal@nasa.gov (N.P. Bansal).

http://dx.doi.org/10.1016/j.ceramint.2014.11.072
0272-8842/Published by Elsevier Ltd and Techna Group S.r.l.

2. Experimental methods

2.1. Glass melting

Desert sand from a Middle East country was melted into glass in a Pt crucible using a programmable box furnace. As-received sand was heated at a rate of 10 °C/minute with isothermal holds of 30 min each at 150 °C, 790 °C, and 1275 °C. After holding at 1500 °C for about an hour for homogenization of the melt, it was quenched in water. The resulting glass frit was ground to powder in a Fritsch Planetary Mill (Model# LC 106- A) using corundum grinding bowl and zirconia milling media.

2.2. Chemical analysis

Chemical composition of the glass powder was analyzed by inductively coupled plasma-atomic emission spectrometry (ICP-AES) using a Varian Vista Pro model in the axial configuration. About 100 mg of glass powder was fused with one gram of sodium carbonate to convert it into soluble form. A reagent blank was carried through the procedure to subtract out impurities from sodium carbonate, particularly the alkali metals. A qualitative scan was done to determine the major and minor constituents. This was followed by a quantitative analysis by comparison with standards of known concentration to create calibration curves for each of the desired elements.

2.3. Hot pressing

The glass powder was loaded into a graphite die and hot pressed in vacuum at ~800 °C under 17 MPa (2.5 ksi) for 10–15 min into discs and bars using a Centorr mini hot press. The applied pressure was released before onset of cooling. Grafoil was used as spacers between the samples and the punches.

Surfaces of hot pressed samples were ground and polished to remove residual grafoil. The final finishing was completed with a #500 diamond grinding wheel under the specified condition in accordance with ASTM standard C1161 [7].

2.4. X-ray diffraction

X-ray diffraction (XRD) patterns of the as-received desert sand, CMAS glass powder, hot pressed samples, and glass powder heat-treated at different temperatures were recorded at ambient temperature using a step scan procedure (0.02°/2θ step, count time 0.4 s) on a Bruker D8 Advanced diffractometer equipped with a crystal monochromator employing copper K_α radiation. A commercial software package, HighScore+ (from PANaltyical), was used for identification of crystalline phases. The software is used to identify peak positions and intensities which are then used to search a powder diffraction database (2012 PDF-4+ database produced by the International Centre for Diffraction Data (ICDD)) for potential matches.

The semi-quantitative analysis of XRD data for desert sand was performed using a variation of the Reference Intensity Ratio (RIR) method as implemented in the PANaltyical HighScore+ software program. In the standard RIR method, an approximation of phase composition is derived from the normalized ratios of the strongest (100%) peak of each phase present, where the 100% peak of corundum is used as the normalization factor. In the HighScore+ program, a regression of peak intensities is used instead of just the 100% peak in order to lessen the impact of preferred orientation, which can diminish the accuracy of this method.

2.5. Thermal analysis

Simultaneous differential thermal analysis (DTA) and thermogravimetric analysis (TGA) were carried out using Netzsch STA 409 C system interfaced with a computerized data acquisition and analysis system at heating/cooling rates of 5 or 10 °C/minute in flowing air. The test samples were contained in alumina cups. Glass transition and crystallization peak maximum temperatures were obtained from the DTA scans. To evaluate crystallization kinetics of the glass, DTA scans were recorded at various heating rates of 2 to 40 °C/min.

2.6. Dilatometry

Glass transition temperature, softening point, and coefficient of thermal expansion (CTE) were measured on a 2.5 cm long hot pressed glass bar using a Netzsch differential dilatometer model 402- C interfaced with a computerized data acquisition and analysis system at a heating rate of 5 °C/min in air. Alumina was used as the standard material.

2.7. Density, elastic modulus, microhardness, and indentation fracture toughness

Density was measured from the bulk mass and volume of the hot pressed disc. Young's modulus, shear modulus, and Poisson's ratio were determined at ambient temperature by the impulse excitation method defined in ASTM C 1259 [8] using the hot pressed glass disc. The test setup records the natural frequency of the disc when excited mechanically in the desired mode. An Audio Technica ATM350 condenser microphone amplified with an M-Audio DMP preamplifier was used to acoustically detect and amplify the natural frequency. A computer system instrumented with National Instruments acoustic signal acquisition hardware and Sound & Vibration Toolset software was used to determine the natural frequency.

Vickers microhardness was evaluated at ambient temperature using hot pressed glass disc with polished surfaces in accordance with ASTM C 1327 [9]. A Zwick model 3212 Hardness Tester was used for the Vickers diamond indent application. The Zwick hardness tester incorporates a dampening mechanism used to lower the indenter which remains in full load contact with the specimen for 15 s. Four different indentation loads of 1.96, 2.9, 4.9, and 9.8 N were used for each series of tests. An upper limit of 9.8 N (1 kg) load was set by the indent exhibiting the start of extreme spalling. A number of indentations were made on the polished specimen

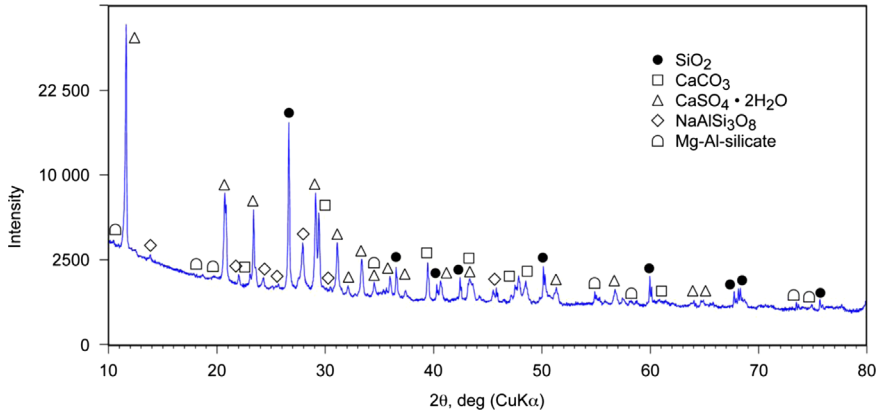

Fig. 1. X-ray diffraction of as-received desert sand from the Middle East showing the presence of $CaSO_4.2H_2O$ (Gypsum), SiO_2 (Quartz), $CaCO_3$ (Calcite), $NaAlSi_3O_8$ (Albite), $Mg_2(Al_{3.9}Si_{5.1}O_{18})$, and $Mg_3Al_2(SiO_4)_3$ phases.

using each load. Indentation diagonal length (2a) and crack length (2c) were measured using the integral optical micrometer for each impression. Values of microhardness and fracture toughness were determined from indentation length and crack length as described earlier [10–12].

3. Results and discussion

3.1. Desert sand

3.1.1. Phase composition

The XRD pattern (Fig. 1) of the as-received desert sand showed the presence of SiO_2 (Quartz), $CaSO_4.2H_2O$ (Gypsum), $CaCO_3$ (Calcite), $NaAlSi_3O_8$ (Albite), and Mg-Al silicate phases. Approximate composition of the desert sand was calculated to be 34% SiO_2 (Quartz), 41% $CaSO_4.2H_2O$ (Gypsum), 11% $CaCO_3$ (Calcite), 7% $NaAlSi_3O_8$ (Albite), and 5% $Mg_2(Al_{3.9}Si_{5.1}O_{18})$ and $Mg_3Al_2(SiO_4)_3$ phases from semi-quantitative analysis of XRD results.

3.1.2. Thermal stability

Simultaneous DTA/TGA scans of the as-received desert sand at heating/cooling rates of 5 °C/minute in air from room temperature to 1420 °C are shown in Fig. 2. Several thermal events are present. The endothermic peak in DTA at ~155 °C that is accompanied by a weight loss of ~9.68% is due to the dehydration of $CaSO_4.2H_2O$ into $CaSO_4$. The next endothermic DTA event at ~797 °C along with a weight loss of ~6.4% in TGA is ascribed to the decomposition reaction: $CaCO_3 \rightarrow CaO + CO_2$. Endothermic DTA peaks at 1214 and 1282 °C and corresponding weight loss of ~18% in TGA are probably due to the stepwise decomposition of $CaSO_4$ according to the reactions: $CaSO_4 \rightarrow CaSO_3 + ½\ O_2$ followed by $CaSO_3 \rightarrow CaO + SO_2$. The exothermic peak at 1344 °C may be due to the formation of $CaSiO_3$ and/or $CaAl_2Si_2O_8$ phases through solid state reaction(s) between the constituents. Presence of a very broad endotherm during cooling in the DTA indicates the absence of crystallization of the CMAS.

3.2. Glass

3.2.1. Composition

From inductively coupled plasma-atomic emission spectrometry (ICP-AES), chemical composition of the CMAS glass powder was analyzed to be 25.2CaO-2.6MgO- $8.2Al_2O_3$-$59.8SiO_2$-$1.6Fe_2O_3$-$1.5K_2O$ (weight %) or 27.8CaO-4MgO-$5Al_2O_3$-$61.6SiO_2$-$0.6Fe_2O_3$-$1K_2O$ (mole %). Small amounts ($< 0.5\%$) of other oxides (Na_2O, TiO_2) were also detected by ICP but are not listed here. Composition of the desert sand glass of the current study is richer in silica but contains lower amounts of CaO, MgO and Al_2O_3 than the composition 35CaO-10MgO-$7Al_2O_3$-$48SiO_2$ (mole %) of the synthesized model CMAS used by other researchers [1–4].

3.2.2. Crystallization

Simultaneous DTA/TGA scans of the CMAS glass powder recorded at a heating rate of 10 °C/minute in air are given in Fig. 3. The DTA shows a glass transition inflection (T_g) at 734 °C and a couple of exothermic peaks at 878 and 982 °C. The first exothermic peak corresponds to the crystallization of $Ca_2Mg_{0.5}AlSi_{1.5}O_7$ and the second to the precipitation of $CaSiO_3$ phase in the glass as indicated by XRD results later in this section. The crystallization onset temperature, T_x, for this glass is found to be ~880 °C from the DTA curve. No thermal event is observed during the cooling cycle. A large value of 146 °C for (T_x-T_g) indicates this glass to be highly stable. The weight changes observed in TGA during heating and cooling are due to artifact of the instrument because of gas buoyancy effect.

To evaluate crystallization kinetics of the CMAS glass, DTA scans were recorded at various heating rates of 2 to 40 K/min. A typical DTA scan recorded at a heating rate of 20 K/min from room temperature to 1100 °C in air is shown in Fig. 4. Values of peak maximum temperatures (T_p) for the two crystallization peaks at various scan rates are given in Table 1. Duplicate DTA runs were made at the scan rate of 5 K/min. Values of T_{p1} and T_{p2} for the two runs at heating rate of 5 K/min in Table 1 indicate very good reproducibility. Values of T_p are seen to increase with increase in heating rate. The crystallization peak

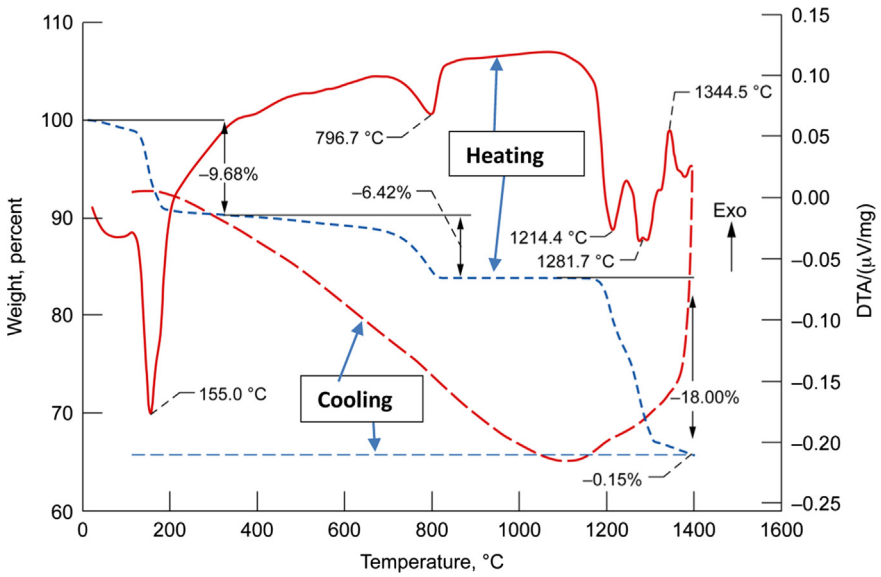

Fig. 2. Simultaneous DTA and TGA of as-received desert sand from the Middle East at heating/cooling rates of 5 K/minute in air.

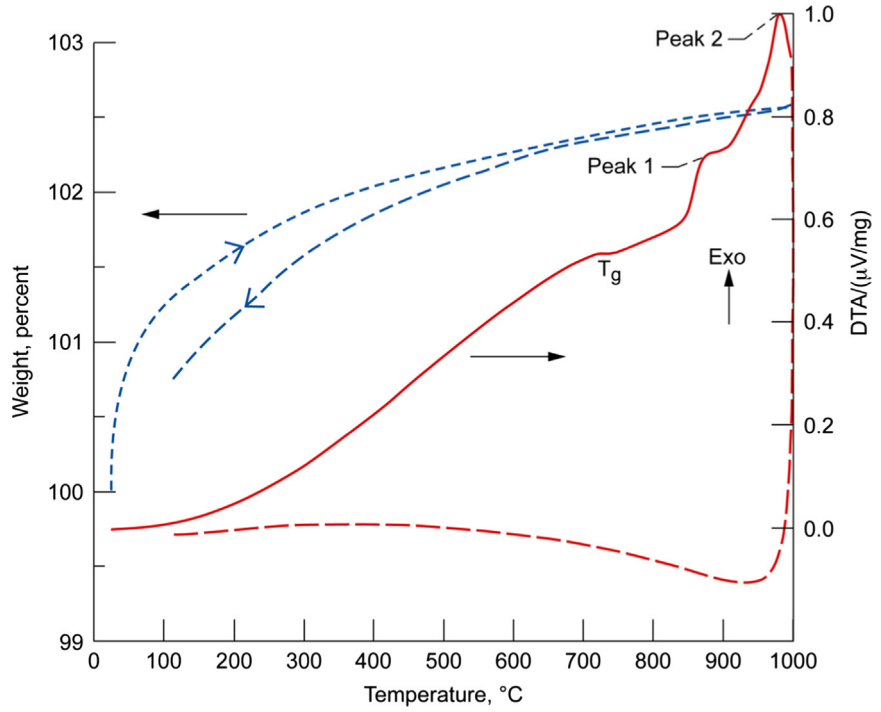

Fig. 3. Simultaneous DTA and TGA of sand CMAS glass powder at heating/cooling rates of 10 K/minute in air.

maximum in the DTA or DSC scans corresponds to the temperature at which the rate of transformation of the viscous liquid into crystals becomes maximum. When the crystalline phase has the same composition as the liquid, the transformation rate will depend on the density of crystallization sites. However, when the composition of the crystalline phase is different from that of the liquid, as in the present case, the rate of transformation will be controlled by the rate of diffusion through the viscous liquid and the number of crystallization sites to which diffusion can occur. If the number of nucleation sites is increased, for example, by using slower heating rates, the peak maximum will occur at a temperature at which the melt viscosity is higher, that is, at a lower temperature. This explains the increase in T_p with the heating rate (Table 1) observed in the present study.

It has been shown earlier that the temperature T_p of the crystallization peak changes with heating rate θ according to the relation [13–18]:

$$\ln(T_p^2/\theta) = \ln(E_c/Rv) + E/RT_p \quad (1)$$

where E_c is the effective overall activation energy for the crystallization process, υ is an effective frequency factor which

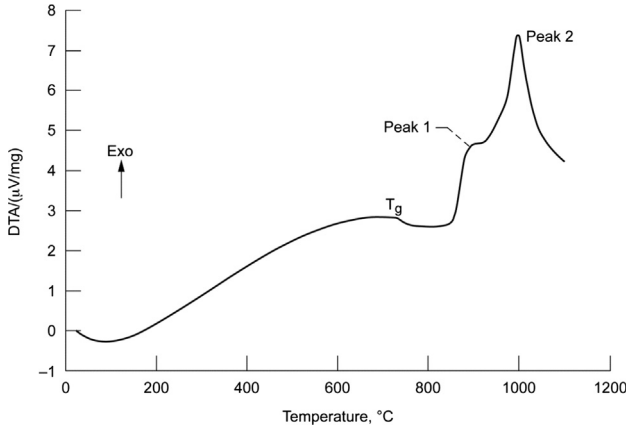

Fig. 4. DTA of desert sand CMAS glass powder at a heating rate of 20 K/minute in air.

Table 1
Effect of heating rate on DTA crystallization peak maximum temperatures (T_p) for desert sand glass.

Scan rate (K/min)	Peak 1 (T_{p1}) (K)	Peak 2 (T_{p2}) (K)
2	1121	1209.8
5	1136	1234.7
5	1136	1234.7
10	1148	1254.9
20	1172	1271.2
30	1188	1280.1
40	1196	1285.9

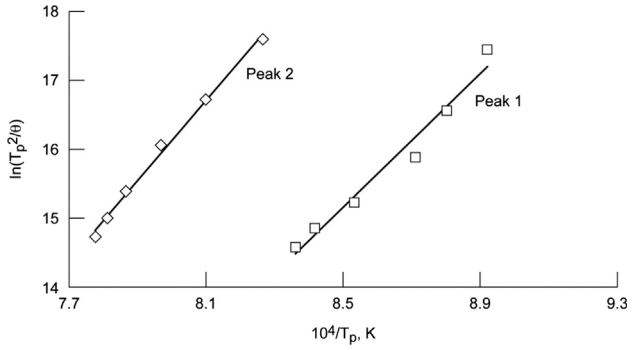

Fig. 5. Plots of ln (T_p^2/θ) versus reciprocal of peak temperature for the two crystallization exotherms for desert sand CMAS glass powder.

is a measure of the probability that a molecule having energy E participates in the transformation, and R is the gas constant. According to eq. (1), a plot of $\ln(T_p^2/\theta)$ versus $1/T_p$ should be linear with a slope of E_c/R and an intercept $[\ln(E_c/R) - \ln \upsilon]$.

Plots of $\ln(T_p^2/\theta)$ versus $1/T_p$ for crystallization of the CMAS glass are shown in Fig. 5. A linear plot indicates validity of the kinetic model of Bansal et al. [13–18] and validity of the assumptions made in this model. Values of kinetic parameters E and υ obtained from linear least squares fitting of the experimental data are listed in Table 2. The crystallization activation energies of 403 and 483 kJ/mol for CMAS glass are in the same range as reported earlier for

Table 2
Kinetic parameters for crystallization of desert sand glass.

Crystallization process	Activation energy, E_c (kJ/mol)	Frequency factor, ν (sec^{-1})
Peak 1	403	9.5×10^{15}
Peak 2	483	9.5×10^{17}

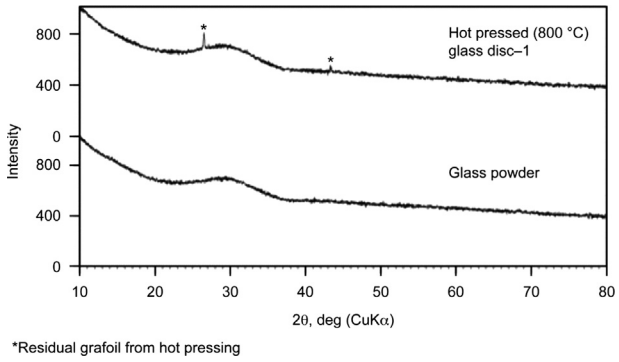

Fig. 6. X-ray diffraction of desert sand CMAS glass powder and glass disc hot pressed at 800 °C for 10 min under 2.5 ksi in vacuum.

barium aluminosilicate (BAS) [16,17] and magnesium aluminosilicate (MAS) [19] glasses.

The XRD pattern of the glass powder is shown in Fig. 6. It contains only a large halo indicating the glass powder to be amorphous, as expected. XRD patterns of CMAS glass powder heat treated at various temperatures from 700 to 980 °C for 10 h. in air are presented in Fig. 7. The results for the development of crystalline phases in the CMAS glass after heat treatments at different temperatures are summarized in Table 3. The glass powder remains amorphous at temperatures up to 850 °C. However, two very minor peaks are present in the XRD of glass heated at 850 °C indicating the initiation of crystallization of $CaSiO_3$. Glass heated at 870 °C is mostly amorphous but contains small crystallization peaks due to the formation of minor amounts of $Ca_2Mg_{0.5}AlSi_{1.5}O_7$ as well as trace amount of $CaSiO_3$ phase. Strong crystallization peaks are observed in the XRD patterns of glass heated at 900 or 980 °C. Glass heated at 900 °C shows the formation of $Ca_2Mg_{0.5}AlSi_{1.5}O_7$ as major phase and $CaSiO_3$ minor crystalline phase whereas $CaSiO_3$ is the major crystalline phase and $Ca_2Mg_{0.5}AlSi_{1.5}O_7$ minor phase in the glass after heating at 980 °C. X-ray diffraction pattern from the surface of a glass disc hot pressed at 800 °C is shown in Fig. 6. The sample is amorphous. The two low intensity peaks are from the presence of residual grafoil on the sample surface.

3.2.3. Dilatometry

Dilatometric thermal expansion curve for a hot pressed one inch long glass bar, measured from room temperature to 820 °C at a scan rate of 5 °C per minute, is shown in Fig. 8. This shows a glass transition temperature (T_g) of 706 °C and dilatometric softening point (T_d) of 764 °C. The average linear

coefficient of thermal expansion (CTE), α, was calculated to be 9.8×10^{-6}/°C in the temperature range from 25 to 700 °C.

3.2.4. Temperature dependence of glass viscosity

Temperature dependence of glass viscosity (η) is expressed by the Vogel-Fulcher-Tamman (VFT) eq. [20]:

$$\log \eta = A + B/(T - T_o) \quad (2)$$

where A, B, and T_0 are constants. Melting point T_m of glass is estimated from Bemann eq. [21]:

$$T_g/T_m = 2/3 \quad (3)$$

For silicate glasses, a number of specific viscosity values have been assigned as reference points corresponding to various temperatures. For silicate glasses, viscosity values at reference temperatures T_g, T_d, and T_m are designated as $10^{13.6}$, $10^{11.3}$, and 10^6 dPaS, respectively [22]. For the sand glass of the present study, values of T_g, T_d, and T_m are 979, 1037, and 1468.5 K. Values of constants A, B, and T_0 of VFT eq. (1) are determined from three equations by substituting η values corresponding to T_g, T_d, and T_m in eq. (2). For sand glass, values of these constants are calculated to be: A = 2.6 kPa.s, B = 2418 kPa.s.K, and T_0 = 759 K.

The VFT equation for the desert sand glass becomes:

$$\log \eta = 2.6 + 2418/(T - 759) \quad (4)$$

Temperature dependence of viscosity of the desert sand glass based on eq. (4) is shown in Fig. 9. Giordano et al. [23] have presented a model to calculate the viscosity of silicate melts as a function of temperature from the melt chemical composition. A web based calculator is also available [24] for calculations of glass viscosity and glass transition temperature T_g. Temperature dependence of desert sand glass viscosity calculated from its composition based on Giordano's model is shown in Fig. 9 and could be expressed by the relation:

$$\log \eta = -4.55 + 7456.3/(T - 570.9) \quad (5)$$

The agreement between the viscosity values calculated by the two methods as seen from Fig. 9 is reasonable at lower temperatures but not so good at high temperatures. Also, the value of T_g calculated from this model was 748.4 °C which is much higher than the experimental value of 706 °C.

3.2.5. Density, elastic modulus, microhardness, and indentation fracture toughness

Bulk density of CMAS glass was determined to be 2.69 g/cm^3 from weight and volume measurements. Values of Young's modulus (E), Shear modulus (G), and Poisson's ratio (σ) were measured to be 92.3 GPa, 36 GPa, and 0.28 respectively.

For Vickers microhardness measurements, a number of indentations were made on the surface of a hot pressed polished specimen using indentation loads of 1.96, 2.9, 4.9,

Table 3
Development of crystalline phases in desert sand glass after heat treatments at various temperatures for 10 h in air.

Sample	Temperature (°C)	Phases from XRD
SG-700	700	Amorphous
SG-800	800	Amorphous
SG-850	850	Amorphous
SG-870	870	$Ca_2Mg_{0.5}AlSi_{1.5}O_7$, $CaSiO_3$
SG-900	900	$Ca_2Mg_{0.5}AlSi_{1.5}O_7$, $CaSiO_3$
SG-980	980	$CaSiO_3$, $Ca_2Mg_{0.5}AlSi_{1.5}O_7$

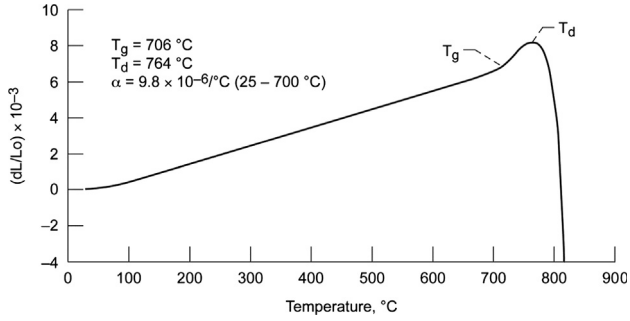

Fig. 8. Dilatometric thermal expansion scan of hot pressed desert sand CMAS glass at a heating rate of 5 °C/minute in air.

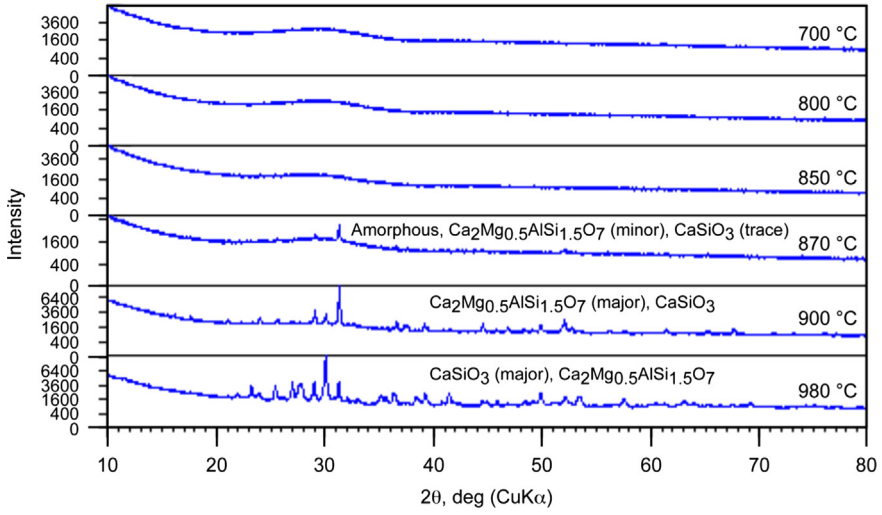

Fig. 7. X-ray diffraction of desert sand CMAS glass powder heat treated at various temperatures for 10 h. in air.

and 9.8 N. Typical indentations on the glass specimen at various loads are shown in Fig. 10. An upper limit of 9.8 N (1 kg) load was set by the indent exhibiting the start of extreme spalling. Indentation diagonal length (2a) and crack length (2c) were measured for each impression. Results for an indentation were not included if value of c/a was less than 2.3 or if crack branching was present. Vickers microhardness was calculated using the equation:

$$H_v = 1.854\left[P/(2a)^2\right] \quad (6)$$

where H_v is the Vickers microhardness in Pascal, P is the applied load in Newton, and 2a is the indent diagonal length in meter. Values of H_v at various loads are shown in Table 4. Average value of H_v for the desert sand glass was found to be

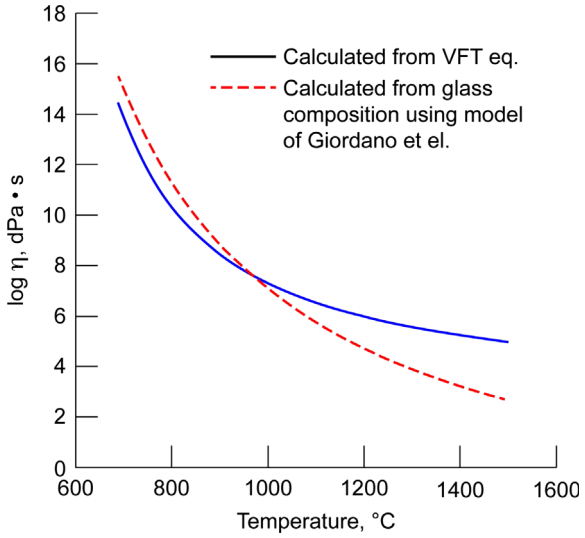

Fig. 9. Temperature dependence of viscosity of desert sand CMAS glass (a) solid line calculated from VFT eq. using viscosity values corresponding to glass reference points and (b) broken line calculated from glass composition using model of Giordano et al. [23,24].

Table 4
Vickers hardness and indentation fracture toughness of desert sand glass.

Indent load (N)	Crack length (2c)/Indent length (2a)	Vickers hardness, H_v (GPa)	Indentation fracture toughness, K_c ($MPa.m^{1/2}$), from various equations		
			Eq.(7) Miyoshi et al.	Eq.(8) Marshall & Evans	Eq.(9) Anstis et al.
1.96	2.9 ± 0.05	5.9 ± 0.1	0.7 ± 0.03	0.7 ± 0.03	0.6 ± 0.03
2.94	2.8 ± 0.1	6.6 ± 0.1	0.8 ± 0.05	0.9 ± 0.1	0.7 ± 0.05
4.9	3.2 ± 0.1	6.4 ± 0.1	0.75 ± 0.05	0.8 ± 0.1	0.65 ± 0.05
9.8	3.8 ± 0.2	6.2 ± 0.1	0.65 ± 0.05	0.7 ± 0.1	0.6 ± 0.1

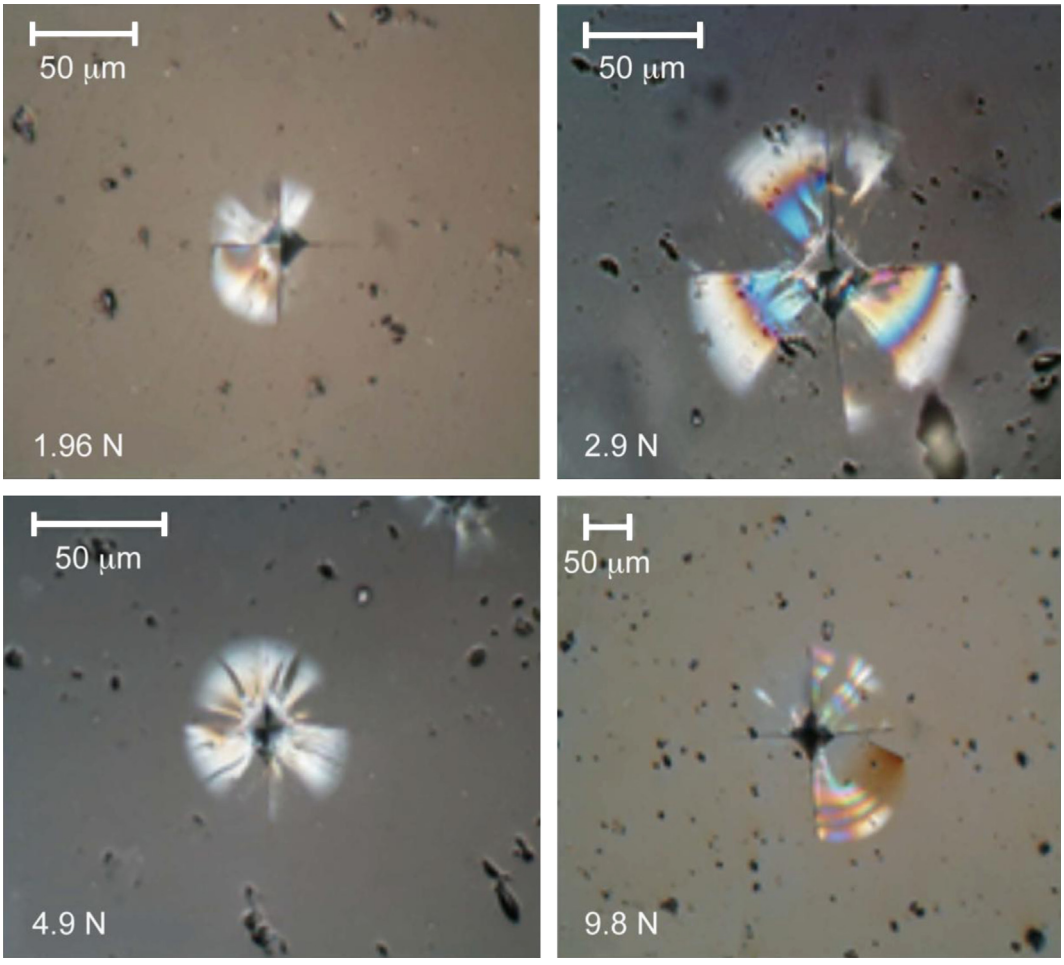

Fig. 10. Optical micrographs showing Vickers indentations on CMAS glass at applied loads of (a) 1.96 N, (b) 2.9 N, (c) 4.9 N, and (d) 9.8 N.

6.3 ± 0.4 GPa. This value of Vickers microhardness for desert sand glass falls in the same range as found for other silicate glasses.

A number of mathematical equations are available for determination of indentation fracture toughness [25–29]. Miyoshi et al. [25] provided the relation:

$$K_c = 0.0264E^{0.5}P^{0.5}a/c^{-1.5} \quad (7)$$

where K_c is the indentation fracture toughness in MPa.m^{½}, E is the Young's modulus in GPa, P is the indentation load in Newton, a is the half indent length in meter, and c is the half crack length in meter. Marshall and Evans [26] reported the following relation:

$$K_c = 0.036E^{0.4}P^{0.6}a^{0.8}c^{-1.5} \quad (8)$$

for evaluation of K_c. According to Anstis et al. [27], K_c may be obtained from the equation:

$$K_c = \beta P\left(E/H_v\right)^{1/2}c^{-1.5} \quad (9)$$

where β is an empirical constant. Based on a fit to experimental data using independent fracture toughness measurements, Anstis et al. [27] determined the value of β as 0.016 ± 0.004. Values of K_c determined using various eqs. 7 to 9 are listed in Table 4 which are found to be in good agreement with each other. For desert sand glass an average value of indentation fracture toughness was found to be 0.75 ± 0.15 MPa.m^{½} which is typical as found for other silicate glasses. It will be interesting to compare these values with those obtained from the single edge V-notch beam (SEVNB) method.

4. Summary and conclusions

As-received desert sand from the Middle east consisted of quartz (SiO_2), calcite ($CaCO_3$), gypsum ($CaSO_4.2H_2O$), NaAlSi$_3$O$_8$, $Mg_2(Al_{3.9}Si_{5.1}O_{18})$ and $Mg_3Al_2(SiO_4)_3$ phases and showed weight loss of ~35% due to decomposition of $CaCO_3$ and $CaSO_4.2H_2O$ when heated to 1400 °C. Chemical composition of the glass, obtained by melting of desert sand at ~1500 °C, was analyzed to be 27.8CaO-4MgO-5Al_2O_3-61.6SiO_2-0.6Fe_2O_3-1K_2O (mole %) using inductively coupled plasma-atomic emission spectrometry. The glass remained amorphous after heat treating at 850 °C for 10 h but crystallized into $CaSiO_3$ and $Ca_2Mg_{0.5}AlSi_{1.5}O_7$ phases at 900 °C or higher temperatures. Various physical, thermal, and mechanical properties of the glass have been evaluated. The glass showed bulk density 2.69 g/cm^3, Young's modulus 92 GPa, Shear modulus 36 GPa, Poisson's ratio 0.28, dilatometric glass transition temperature (T_g) 706 °C, softening point (T_d) 764 °C, Vickers microhardness 6.3 ± 0.4 GPa, indentation fracture toughness 0.75 ± 0.15 MPa.m$^{1/2}$, and coefficient of thermal expansion (CTE) 9.8×10^{-6}/°C in the temperature range 25 to 700 °C. Temperature dependence of viscosity of the CMAS glass has been estimated from viscosity values at various reference points as well as from the glass composition. Crystallization kinetics of the CMAS glass was also investigated by differential thermal analysis (DTA). Activation energies for crystallization of two different phases in the glass were calculated to be 403 and 483 kJ/mol, respectively. Results reported here will be useful in understanding and modeling the CMAS interactions with thermal and environmental barrier coatings.

Acknowledgments

Desert sand was supplied by NAVAIR. Thanks are due to Dr. Paul Angel, Dr. Richard Rogers, Dr. Valerie Wiesner, Doug Doza, Ralph Pawlik, Derek Johnson, Bob Angus, and Ray Babuder for technical assistance during this work. This research was supported by NASA's Aeronautical Sciences Project as well as by NAVAIR through a space act agreement (SAA3-1260).

References

[1] B.J. Harder, J. Ramirez-Rico, J.D. Almer, K.N. Lee, K.T. Faber, Chemical and mechanical consequences of environmental barrier coating exposure to calcium-magnesium-aluminosilicate, J. Am. Ceram. Soc. 94 (2011) S178–S185.
[2] C. Mercer, S. Faulhaber, A.G. Evans, R. Darolia, A delamination mechanism for thermal barrier coatings subject to calcium-magnesium-alumino-silicate (CMAS) infiltration, Acta Mater. 53 (2005) 1029–1039.
[3] J. Liu, L. Zhang, Q. Liu, L. Cheng, Y. Wang, Calcium-magnesium-aluminosilicate corrosion behaviors of rare-earth disilicates at 1400 °C, J. Eur. Ceram. Soc. 33 (2013) 3419–3428.
[4] U. Schulz, W. Braue, Degradation of $La_2Zr_2O_7$ and other novel EB-PVD thermal barrier coatings by CMAS (CaO-MgO-Al_2O_3-SiO_2) and volcanic ash deposits, Surf. Coat. Tech. 235 (2013) 165–173.
[5] X. Chen, Calcium-magnesium-alumina-silicate (CMAS) delamination mechanisms in EB-PVD thermal barrier coatings, Surf. Coat. Tech. 200 (2006) 3418–3427.
[6] N.L. Ahlborg, D. Zhu, Calcium-magnesium aluminosilicate (CMAS) reactions and degradation mechanisms of advanced environmental barrier coatings, Surf. Coat. Tech. 237 (2013) 79–87.
[7] C. ASTM, Annual Book of ASTM Standards, Vol 15.01, ASTM, West Conshohocken, PA, 2006 (1161).
[8] ASTM C1259, Standard Test Method for Dynamic Young's Modulus, Shear Modulus, and Poisson's Ratio for Advanced Ceramics by Impulse Excitation of Vibration, Vol. 15.01, American Society for Testing and Materials, West Conshohocken, PA, 2001 (Annual Book of ASTM Standards).
[9] C. ASTM, Annual Book of ASTM Standards, Vol 15.01, ASTM, West Conshohocken, PA, 2006 (1327).
[10] N.P. Bansal, J.B. Hurst, S.R. Choi, Boron nitride nanotubes-reinforced glass composites, J. Am. Ceram. Soc. 89 (2006) 388–390.
[11] S.R. Choi, N.P. Bansal, A. Garg, Mechanical and microstructural characterization of boron nitride nanotubes-reinforced SOFC seal glass composite, Mater. Sci. Eng. A 460-461 (2007) 509–515.
[12] S.R. Choi, N.P. Bansal, Mechanical properties of SOFC seal glass composites, Ceram. Eng. Sci. Proc 26 (2005) 275–283.
[13] N.P. Bansal, R.H. Doremus, Determination of reaction kinetic parameters from variable temperature DSC or DTA, J. Therm. Anal 29 (1984) 115–119.
[14] N.P. Bansal, R.H. Doremus, A.J. Bruce, C.T. Moynihan, Kinetics of crystallization of ZrF_4-BaF_2-LaF_3 glass by differential scanning calorimetry, J. Am. Ceram. Soc. 66 (1983) 233–238.
[15] N.P. Bansal, A.J. Bruce, R.H. Doremus, C.T. Moynihan, The influence of glass composition on the crystal growth kinetics of heavy metal fluoride glasses, J. Non-Cryst. Solids 70 (1985) 379–396.
[16] N.P. Bansal,, M.J. Hyatt, Crystallization kinetics of barium aluminosilicate glasses, J. Mater. Res. 4 (1989) 1257–1265.

[17] M.J. Hyatt, N.P. Bansal, Crystal growth kinetics in $BaO.Al_2O_3.2SiO_2$ and $SrO.Al_2O_3.2SiO_2$ glasses, J. Mater. Sci. 31 (1996) 172–184.
[18] N.P. Bansal, E.A. Gamble, Crystallization kinetics of a solid oxide fuel cell seal glass by differential thermal analysis, J. Power Sources 147 (2005) 107–115.
[19] D. Bahadur, N. Lahl, K. Singh, L. Singheiser, K. Hilpert, Influence of nucleating agents on the chemical interaction of $MgO\text{-}Al_2O_3\text{-}SiO_2\text{-}B_2O_3$ glass sealants with components of SOFCs, J. Electrochem. Soc. 151 (2004) A558–A562.
[20] A.K. Varshneya, Fundamental of Inorganic Glasses, Academic Press, New York, 1994, p. 188.
[21] R.G. Beman, F.B. Cramer, Polymer characterization: a typical copolyamide system, J. Polym. Sci 21 (1956) 223–235.
[22] N.P. Bansal, R.H. Doremus, Handbook of Glass Properties, Academic Press, New York, 1986.
[23] D. Giordano, J.K. Russell, D.B. Dingwell, Viscosity of magmatic liquids: a model, Earth Planet. Sci. Lett 271 (2008) 123–134.
[24] ⟨http://www.eos.ubc.ca/~krussell/VISCOSITY/grdViscosity.html⟩.
[25] T. Miyoshi, N. Sagawa, T. Sassa, Study on fracture toughness evaluation for structural ceramics, T. Jpn. Soc. Mech. Eng. 51A (1985) 2487–2489.
[26] D.B. Marshall, A.G. Evans, Reply to comment on elastic/plastic indentation damage in ceramics: the median/radial crack system, J. Am. Ceram. Soc. 64 (1981) C182–C183.
[27] G.R. Anstis, P. Chantikul, B.R. Lawn, D.B. Marshall, A critical evaluation of indentation techniques for measuring fracture toughness: I, direct crack measurements, J. Am. Ceram. Soc. 64 (1981) 533–538.
[28] G.D. Quinn, J. Salem, I. Bar-on, K. Cho, M. Foley, H. Fang, Fracture toughness of advanced ceramics at room temperature, J. Res. Natl. Inst. Stand. 97 (1992) 579–607.
[29] G.D. Quinn, R.C. Bradt, On the vickers indentation fracture toughness test, J. Am. Ceram. Soc. 90 (2007) 673–680.